

Adrian Truszkiewicz, David Aebisher, Dorota Bartusik-Aebisher

Medical Faculty, University of Rzeszow, Rzeszow, Poland

Assessment of spin-lattice T_1 and spin-spin T_2 relaxation time measurements in breast cell cultures at 1.5 Tesla as a potential diagnostic tool in vitro

Corresponding author:

Dorota Bartusik-Aebisher,
University of Rzeszow, Rzeszow,
Poland,
e-mail: dbartusik-aebisher@ur.edu.pl

Medical Research Journal 2020;
Volume 5
10.5603/MRJ.a2020.0005
Copyright © 2020 Via Medica
ISSN 2451–2591

ABSTRACT

Magnetic resonance imaging (MRI) is a critically important tool in current medicine. This dynamic diagnostic method allows for detailed and accurate imaging of the human body and diagnosis of metabolic changes by magnetic resonance spectroscopy (MRS) assays. Our work presented herein shows measurement of spin-lattice T_1 and spin-spin T_2 relaxation time as an indicator of changes in cellular morphology. MRI spin-lattice T_1 and spin-spin T_2 relaxation time measurements are innovative experiments that provide a detailed picture of the biological microenvironment within cell cultures. Here, we used two types of cell cultures: cancerous and healthy breast cells. By measuring spin-lattice T_1 and spin-spin T_2 relaxation time in cancerous and healthy cell cultures we can detect differences and morphological conditions of both cell lines. A number of observations indicate that MRI can detect differences between cancer and healthy cells. In order to obtain a high density of cells for our cellular MRI study, we grew the cells in 3D geometry. In this paper, we underline the potential of quantitative MRI *in vitro* for future cellular mapping of drug concentration and drug efficiency in cell culture. We have shown that MRI, which is used often for imaging of anatomy, is also a promising technology for specific morphological measurements of cells.

Key words: magnetic resonance imaging, cell cultures, spin-lattice T_1 , spin-spin T_2 relaxation time

Introduction

The phenomenon of magnetic resonance imaging (MRI) is based on the interaction of strong magnetic field elements as well as electromagnetic waves at a precisely defined frequency on nuclei. Speaking of magnetic resonance imaging in the sense of diagnostic imaging, we are usually talking about imaging of ^1H hydrogen nuclei. The phenomenon itself was described for the first time by its discoverer I. I. Rabi in his publication concerning new methods of measuring magnetic moments [1]. Since then, the world has entered an era of diagnostics at the molecular level.

This phenomenon uses the influence of an electromagnetic wave with a strictly defined frequency – called a resonance frequency (f_0) – on hydrogen nuclei placed in a strong magnetic field. This frequency depends linearly on the value of the magnetic field induction B_0 in which the sample is placed and on the gyromagnetic constant, the value of which is characteristic for a given

element. This frequency is described by the Larmor equation

$$f_0 = \frac{1}{2\pi} \gamma B_0 \quad \text{Equation 2}$$

f_0 — resonant frequency

γ — gyromagnetic constant

B_0 — magnetic field induction value

Relaxation time T_1 is the time for longitudinal magnetisation to return to the Z axis at 63% of the original state. This relaxation is called the spin-lattice relaxation time because in the process of return, energy is transferred to the lattice. Due to the fact that the Z component is being rebuilt, the time T_1 is also called the longitudinal relaxation time and is dependent on temperature. The speed of the process depends on the force with which protons interact with the environment, and the faster it is, the more macromolecules are found in the examined tissue. The longest T_1 times occur for tissues with the highest water content and the lowest macromolecule content [2].

MRI is primarily associated with the study of the human body. This environment is relatively stable when it comes to temperature changes inside. It is different for other studies, and in particular, for cell cultures where cell growth itself takes place at 37°C, whereas the test is carried out at lower temperatures. In order to minimise errors in determining relaxation times, the temperature of the tested samples should be stabilised. The effect of temperature on relaxation time T_1 is known [3]. For water, the relaxation time T_1 increases with increasing temperature. This time also depends on the viscosity of the environment. The presence of magnetic nuclei is an important factor influencing this parameter. The presence of paramagnetic nuclei in the sample causes a reduction of T_1 time. This phenomenon is used in the design of contrast agents based on elements such as gadolinium. The relaxation time T_2 is the time needed for transverse magnetisation to reach 37% of the initial value. T_2 time is associated with the loss of spin coherence, i.e. with their phasing. The phenomenon of phase coherence depends on the tested object itself but also on the parameters of the magnetic resonance system. In particular, the parameter is affected by the homogeneity of the B_0 field. The heterogeneity of the field means that individual nuclei are in a different magnetic field. These are usually very small equations but sufficient for protons to have different resonance frequencies. This leads in a straight line to the phase of the system and the disappearance of the transverse component of the magnetic field. The next reason for the decay of the transverse component is the properties of the sample itself. For this reason, lateral relaxation is referred to as spin-spin relaxation.

By choosing the multiplicity of echo time (TE) and repetition time (TR) properly, we can highlight the differences between selected tissues. In general, the magnetic resonance signal obtained by the receiving coils can be described by Equation 2 (spin echo sequence has been considered).

$$IS \approx PD \left(1 - e^{-\frac{TR}{T_1}} \right) e^{-\frac{TE}{T_2}} \quad \text{Equation 2}$$

PD — proton density in tissue

T_1 — longitudinal relaxation time tissue

T_2 — transverse relaxation time tissue

TE — echo time

TR — repetition time

Analysing the above equation, we can see that we are dealing with relatively simple relationships in which there are three parameters depending on the test centre proton density (PD), T_1 , T_2 , and those given by the system operator (TE, TR). Medical images are obtained during the test with TE and TR parameters set. Choosing them properly enables the scanner operator to change the image allowing better or worse visualisation of individual anatomical structures. Each T_1 -dependent and T_2 -dependent image is created with TE and TR times assumed in advance. Table 1 summarises the individual values of T_1 and T_2 times, which, when taken into account in the test sequences, allow imaging of selected areas of the human body [4, 5].

Material and methods

All MRI measurements were made on the OPTIMA 360 magnetic resonance system (General Electric Health Care) with a field induction of 1.5 Tesla. Human mammary epithelial cells and MCF-7 cell lines for further culture and research and culture media were obtained from the American Type Culture Collection (Manassas, VA, USA).

Cell cultures

Human MCF-7 cell line was obtained from the American Type Culture Collection (Manassas, VA,

Table 1. Water content in tissue with corresponding T_1 and T_2 times at 1.5 Tesla [4, 5]

Tissue	Water content [%]	T_1 [ms]	T_2 [ms]
Grey matter of the brain	84	920	101
White matter of the brain	71	780	76
Cerebrospinal fluid	97	3270	1660
Skeletal muscle	79	860	47
Heart	80	860	57
Liver	71	620	43
Kidney	81	1220	58
Spleen	79	1070	62
Subcutaneous fat	-	230	85

Table 2. The composition of samples A–E shown in Figure 2

	Sample A	Sample B	Sample C	Sample D	Sample E
Sample composition	10 ml H ₂ O + 1.063 g CuSO ₄ → C _m = 0.666 mol/l	9 ml H ₂ O + 1 ml of sample A → C _m = 0.0666	9 ml H ₂ O + 1 ml of sample B → C _m = 0.00666	9 ml H ₂ O + 1 ml of sample C → C _m = 0.00066	H ₂ O
T ₁	43 ms	310 ms	1109 ms	2110 ms	2637 ms
T ₂	25 ms	227 ms	696 ms	1001 ms	1337 ms

USA). HER-2 overexpression of these cell lines was confirmed with cytometric analysis. The CO₂-independent medium was supplemented with 10% buffered foetal bovine serum (FBS), 1% l-glutamate, and 1% antibiotic (penicillin/streptomycin). Prior to maintenance in a hollow-fibre bioreactor (HFB), the passaged cells were re-suspended in CO₂-independent medium and plated (25 mL, 1×10⁶ cells/mL) on a six-well tissue culture polystyrene (TCPS) plate. Each well was then filled with 2 mL of the CO₂-independent medium and cultured at 37°C under atmospheric pressure CO₂ for 24 h. The cells were maintained in tissue culture flasks and were cultured as monolayers until the number of cells reached 0.5×10⁵ cells/mL. MCF-7 cell cultures were grown for four weeks.

Human mammary epithelial cells (HMEC) (GIBCO Invitrogen, Rockville, MD) were isolated from mammo-plastic tissue and cultured in a culture flask until the number of cells reached 0.5×10⁵ cells/mL. The Medium 171 supplemented with 0.4% bovine extract, 5 mg/L bovine insulin, 0.5 mg/L hydrocortisone, and 3μg/L human epidermal growth factor were used.

Phantom measurements

All measurements were made on an OPTIMA 360 magnetic resonance system GEHC with a field induction of 1.5 Tesla. The basic parameters of the gradient system, which are the amplitude and growth rate, are 33 mT/m and 120 T/m/s, respectively. This work was also performed in part to show that methods work on an in vivo clinical machine that is not equipped with specialised or modern functionalities. The measurements were carried out using a surface coil. The choice of the coil was dictated by the very characteristics of the surface coil as well as the size of the objects tested. Surface coils have very good sensitivity at a short distance from their surface. The disadvantage is the fact that the signal intensity drops very quickly as the distance between the tested layer and the receiving elements of the electronic system increases. Four tubes containing different concentrations of CuSO₄ aqueous solution and one sample that contained distilled water were implemented for the experiments. In general, the phantom

contained five tubes. To test tube No. 1 containing 10 ml distilled water was added 0.1063 g of copper sulphate with a molar mass of 159.609 g/mol. This quantity was weighed on an analytical balance. Each subsequent tube contained 9 mL of water and 1 mL of solution from its previous tube number. This resulted in four solutions with significantly different concentrations to illustrate the possibility of measuring changes in T₁ and T₂ time depending on the concentration of CuSO₄ in the sample. The study used the T₁ fast spin echo sequence. TE time was 20 ms while TR times were, respectively, 40 ms, 50 ms, 60 ms, 78 ms, 80 ms, 100 ms, 120 ms, 140 ms, 200 ms, 240 ms, 300 ms, 400 ms, 500 ms, 600 ms, 700 ms, 800 ms, 1000 ms, 1500 ms, 2000 ms, 3000 ms, 5000 ms, 10000 ms, and 15000 ms. Such a large number of measuring points became necessary to determine the wide range of T₁ times that the samples displayed in the study. Increasing the number of measuring points also positively affects the process (Tab. 2), (Fig. 1, 2).

The samples were analysed with MATLAB software. T₁ and T₂ time determination procedure was implemented. The data for analysis came directly from DICOM files generated in the MR system. Figure 1A presents a fragment of the obtained scan of tubes. Test tubes were stowed in a row vertically in the long axis of the magnet. The obtained images are the result of coronal scanning. The prepared samples were arranged in order from the highest concentration – sample a). to the smallest – sample d). The last sample contains distilled water with a conductivity below 8 μS.

Results

Figure 1B shows the time distribution T₁ for the test area. It can be clearly seen that during T₁ it rapidly decreases with increasing CuSO₄ concentration. Table 3 presents the results of measuring T₁ times for each sample separately. The measurement was based on the signal intensity averaged over the sample surface. It should be noted that the longitudinal relaxation time changes rapidly even for a very small amount of copper sulphate. Figure 1C shows the ratio of the approximation curve fitting factor to the measurement

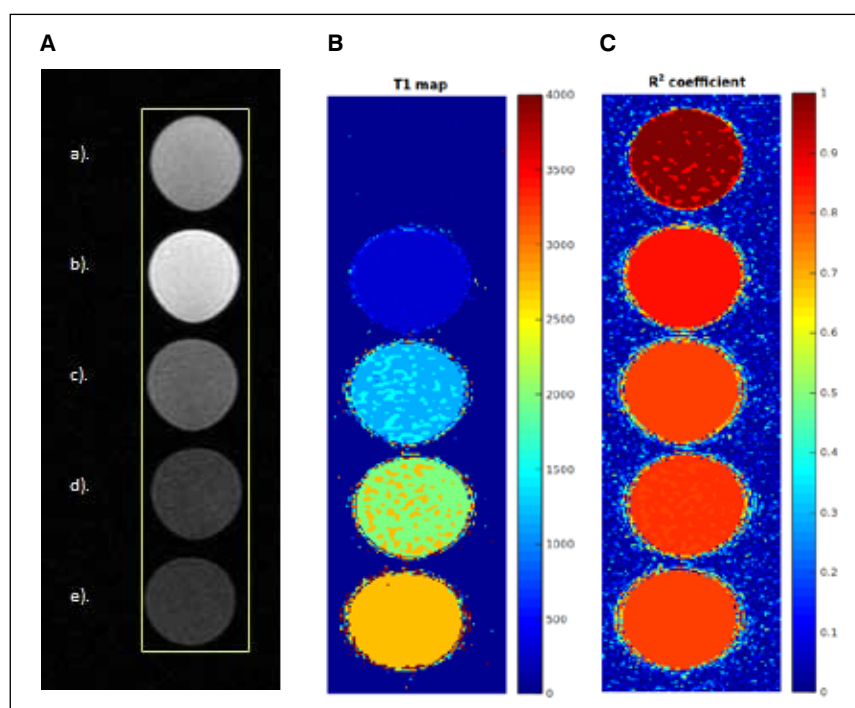


Figure 1. A. sample system during the T₁ measurement, B. T₁ time distribution in tested samples, C. approximation curve fit factor — R²

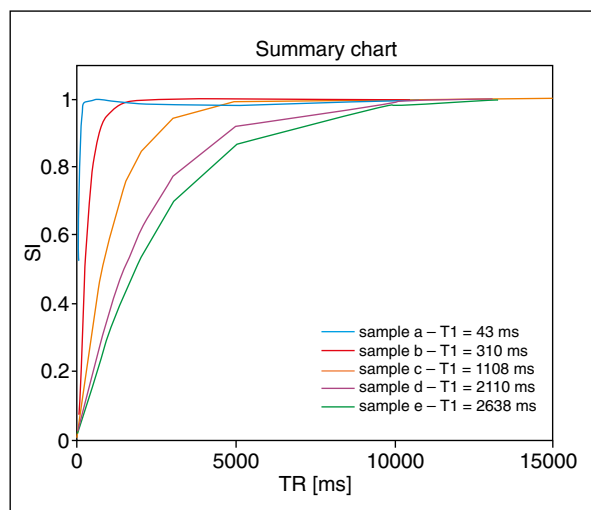


Figure 2. Summary chart of T₁ longitudinal relaxation for five samples a–e

results. It is clear that R² for the sample is around 0.8. Such a high matching result relays information about the accurate estimation of the measured time T₁. Image regions that do not correspond to the sample area have the same factor at a very low level. Best fit was achieved for the shortest T₁ times. The images of the samples contain areas of different times – this is related to noise and interference. The T₁ time value for water was set at 2637 ms.

Figure 3 shows the results of T₂ transverse relaxation time measurements for samples. They were determined by the function implemented in the system; the T2MAP sequence at TR = 640 ms was used for the measurements. However, its use in the unchanged version resulted in a very inaccurate determination of transverse relaxation times. Much better results were achieved when the TR time was changed to 3000 ms.

Relaxation times are burdened with a number of factors that affect their outcome. This time should be at least five times longer than the measured time T₁. The researchers assumed the TR value at the level of 15,000 ms as the maximum time. The choice of such a long time was dictated by the presence of distilled water in one tube. For short times below 2000 ms, a maximum TR value of 10,000 ms can be assumed. Limiting the value of repetition times is crucial to shortening the study time.

Cell culture measurements

Cells from the bioreactor were transferred to tubes to increase their concentration in a small volume. There are many studies in the literature that discuss measuring the relaxation time of cell cultures [6–10]. To determine the T₁ time, the study was carried out in the T₁ FSE sequence. The layer thickness was 3 mm, field of view (FOV) 5 cm, echo time (TE) 10.73 ms, imaging matrix 320×224, and repetition times for subsequent acquired

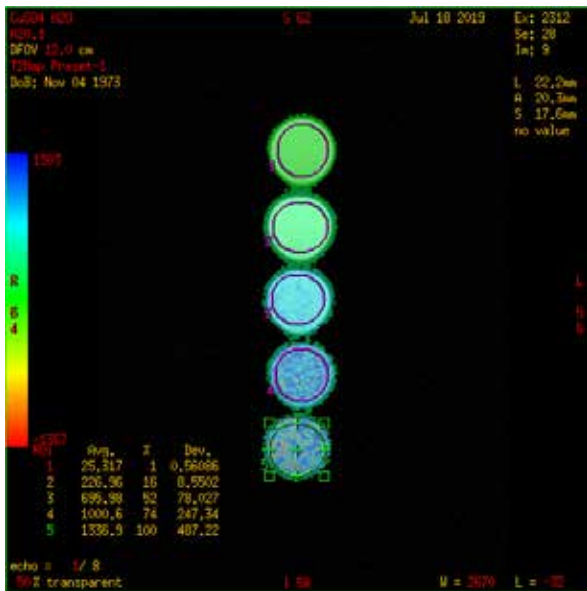


Figure 3. Result of the T2map sequence operation and analysis of the obtained images in the OPTIMA360 magnetic resonance system manufactured by GEHC

sequences were 78 ms, 100 ms, 200 ms, 500 ms, 700 ms, 1000 ms, 1500 ms, 2000 ms, 3000 ms, 5000 ms, 10000 ms, and 15000 ms. Shimming – pre-scan as well as the function of correcting the geometry and signal intensity – was made only for the first sequence due to the need to keep the same system setting parameters. Changing the parameters of the sequence could lead to minor changes in the operation of the apparatus, and this would affect the measured signal. This state of affairs would increase the error.

Figure 4A shows a map of T_1 time value distribution derived for a sample of HMEC cell culture. It was created as a result of calculating the longitudinal relaxation time for each pixel of the image separately. The presented image is a fragment from the entire MR image with dimensions of 45×43 pixels for better imaging of changes. Assuming a FOV of 5 cm and an imaging matrix of 512×512 , one pixel corresponds to 0.097 mm. The image shows significant differences in the value of T_1 time. This is due to the high noise associated with scanning small objects with a surface coil and the heterogeneity of the object. Some noise can be reduced by reducing the matrix. The neighbouring areas are then averaged. The fit quality of the approximation curve is determined by the fit factor R^2 . Figure 4B shows the distribution of the coefficient in the test space, which, for the measured object, is for the majority of the pixel above about 0.79.

Figure 5 presents the results of the average measurement for the sample. The time for the selected area of interest is 2484 ms. In the lower right corner of the

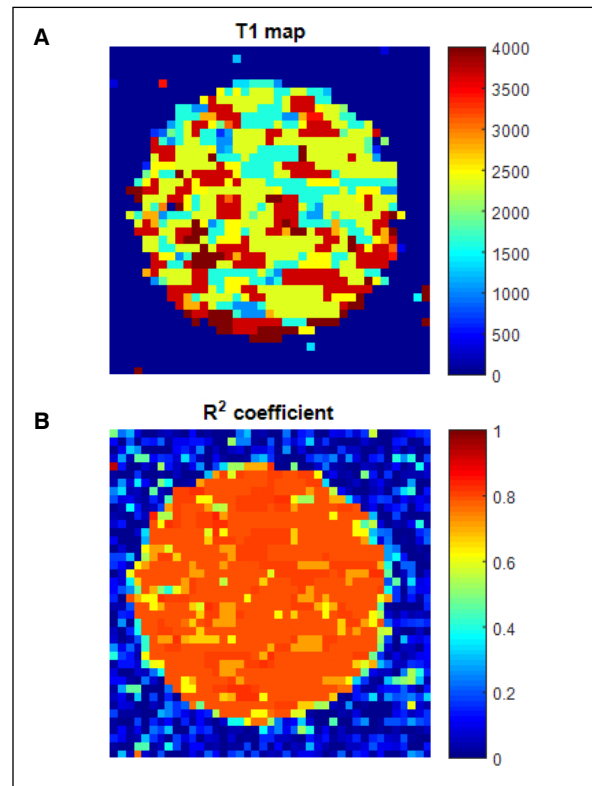


Figure 4. A. distribution map of T_1 time values for a sample of HMEC healthy cell culture, **B.** R^2 fit factor

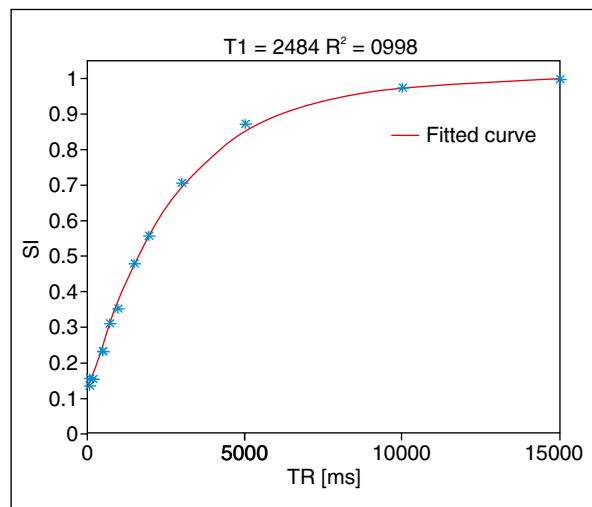


Figure 5. Result of the measurement of longitudinal relaxation time T_1 as an average value for a healthy cell culture sample

graph, there is a section of the image with the averaging area selected.

Figure 6 shows a distribution map of T_1 time values for a sample of MCF-7-derived cell culture and R^2 fit factor.

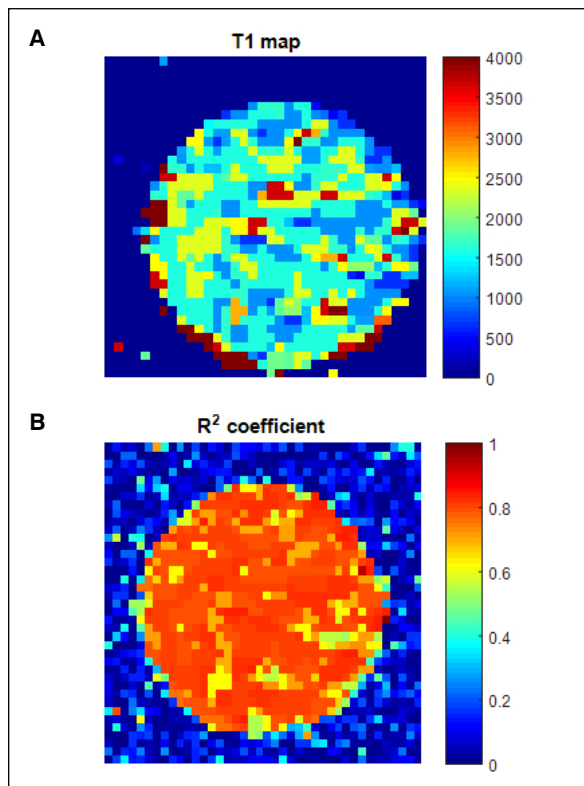


Figure 6. A. distribution map of T1 time values for a sample of MCF-7 — derived cell culture, B. R2 fit factor

Figure 7 presents the result of the average measurement for the sample. This time for the selected area of interest is 1843 ms. As a result of comparing T_1 values for healthy and cancerous tissues, it can be seen that they have significantly different values.

Figure 8 presents the result of scanning cell culture using the unmodified T_2 map sequence available in the OPTIMA 360 camera. As you can see, the image is burdened with a high level of noise, which affects the determination of relaxation time.

Discussion

Relaxation times are the basic parameters that characterise examined objects in magnetic resonance imaging. In recent years, leading manufacturers of magnetic resonance imaging systems have developed a number of applications that illustrate anatomy using relaxation times. Images obtained of the myocardium, brain areas, and neoplastic lesions where the T_1 or T_2 time values are colour coded gave doctors an additional diagnostic tool that significantly influences medical diagnostics. The latest software allows post-processing changes of TE, TR, and TI times, which makes it possible to obtain several images, including parametric images (T_1 , T_2 , STIR, T_1 FLAIR, T_2 FLAIR, PD) in a significantly shorter time [10–16].

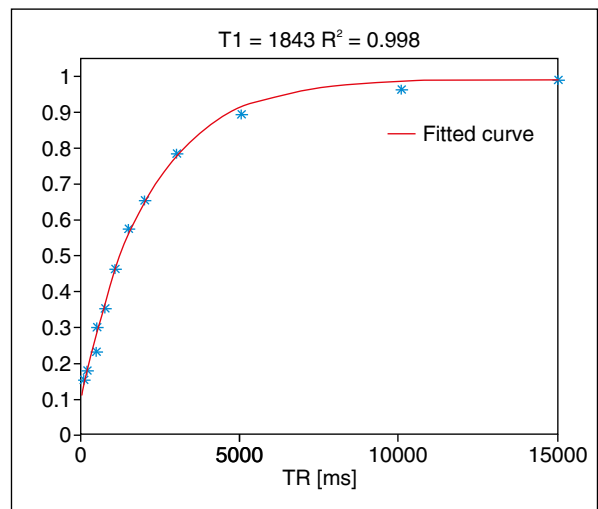


Figure 7. Result of the measurement of T1 longitudinal relaxation time as averaged value for a tumor cell sample

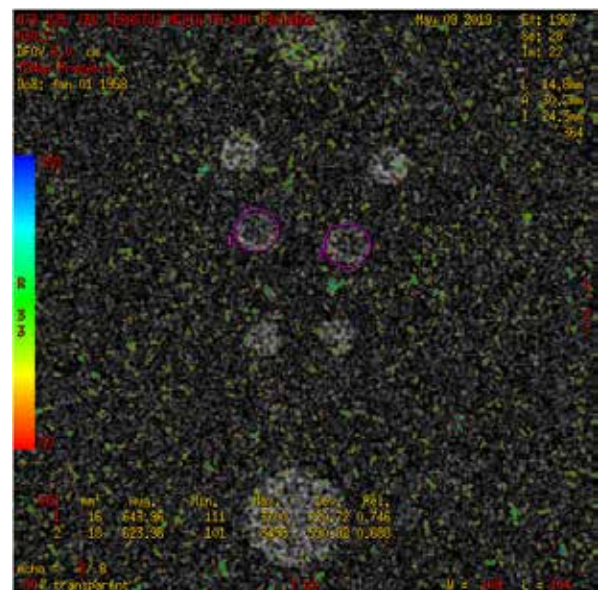


Figure 8. Result of T2 transverse relaxation time measurement for healthy HMEC ROI No. 1 and MCF-7 ROI No. 2 tumor cell culture

Nevertheless, at the core of this technology are the principles of measuring relaxation times with in-depth knowledge of phenomena affecting the accuracy of the results obtained.

The conducted experiments show that the protocols that were created for imaging the structures of the human body do not always give correct results for cell cultures. It is therefore necessary to modify them to select optimal scanning conditions. The second important conclusion is that HMEC tumour cells have a shorter T_1 time compared to the HMEC cell line. Hydrogen is the element most commonly found in the human body.

Table 3. A list of NMR active nuclei with significant parameters

Element	Spin	Gyromagnetic coefficient $\gamma \left[10^6 \frac{\text{rad}}{\text{s} \cdot \text{T}} \right]$	Frequency for 1 T $\frac{\gamma}{2\pi} \left[\frac{\text{MHz}}{\text{T}} \right]$	Frequency for 1.5 T $\frac{\gamma}{2\pi} \left[\frac{\text{MHz}}{\text{T}} \right]$	Frequency for 3 T $\frac{\gamma}{2\pi} \left[\frac{\text{MHz}}{\text{T}} \right]$	Relative sensitivity	Isotope occurrence in nature [%]
1H	1/2	267.5221900(18)	42.57747892(29)	63.86621838	127.73243676	1.00	99.985
2H	1	41.065	6.536	9.804	19.608	1.45×10^{-6}	0.015
3H	1/2	-203.789	-32.434	-48.651	-97.302	5.75×10^{-7}	1.4×10^{-4}
7Li	3/2	103.962	16.546	24.819	49.638	0.272	92.58
13C	1/2	67.2828	10.7084	16.0626	32.1252	1.76×10^{-4}	1.108
14N	1	19.331	3.077	4.6155	9.231	1.00×10^{-3}	99.630
15N	1/2	-27.116	-4.316	-6.474	-12.948	3.86×10^{-6}	0.370
17O	5/2	-36.264	-5.772	-8.658	-17.316	1.08×10^{-5}	0.037
19F	1/2	251.662	40.052	60.078	120.156	0.834	100
23Na	3/2	70.761	11.262	16.893	33.786	9.27×10^{-2}	100
29Si	1/2	-53.190	-8.465	-12.6975	-25.395	3.68×10^{-4}	4,6832
31P	1/2	108.291	17.235	25.8525	51.705	6.65×10^{-2}	100
39K	3/2	12.50	1.989	2.9835	5.967	4.75×10^{-4}	93.100
129Xe	1/2	-73.997	-11.777	-17.6655	-35.331	5.71×10^{-3}	26.44

Approximately 65% of human body weight is water, which, when combined with its magnetic resonance imaging properties, makes it perfect for MRI research. It is endowed with the greatest magnetic moment among solid isotopes. Following Equation 1 and knowing the value of the magnetic field, you can easily determine the resonance frequency of nuclei. Table 3 contains gyromagnetic coefficients for several of the most important chemical elements of importance in medicine. There are also resonance frequencies for individual nuclei depending on the value of magnetic field induction B_0 [16–20].

The phenomenon itself occurs only for those nuclei that have a non-zero spin. For nuclei that do not have spin, magnetic resonance imaging does not occur.

In order to approximate the phenomenon, let us assume that we are dealing with a sample containing a certain amount of hydrogen atoms. In addition to the magnetic field, the spins of individual nuclei have a random direction of rotation, so the resulting magnetic moment of the sample is zero. The situation changes when the sample is placed in a constant magnetic field with B_0 induction. Spins of individual atoms will be ordered according to the direction of the magnetic field. Some of them will accept a consistent return and the remainder are opposite to the return of the field force lines of this constant field and B_0 induction. Research shows that the difference in order is around 45 ppm [21]. The direction parallel or anti-parallel to the direction of the main magnetic field is associated with the level of energy of protons. Protons with higher

energy will position themselves anti-parallel, while those with less energy will be parallel to the magnetic field induction line. The number of atoms arranged in parallel is greater. This small equality is the source of the signal received by the coils. Increasing the magnetic field strength increases the useful signal level, which is associated with a greater difference in the number of energy levels. A similar effect on the signal level is achieved by lowering the sample temperature. In the tested sample, the order of proton spins occurs according to the magnetic field force lines. The sum of all vectors derived from individual atoms makes up the total magnetisation value M_0 [10–15].

The proton rotational motion can be compared to the gyro rotation. Its deflection depends on the intensity of the electromagnetic wave with the Larmor frequency f_0 . At the moment when the wave emitter is turned off, the processing protons will start returning to the state they were in before the beginning of the wave emission. This return is called relaxation and is the basic concept associated with magnetic resonance imaging. For the sake of accuracy, it should be noted that there are two relaxation times: longitudinal and transverse, designated T_1 and T_2 , respectively. In the imaging method described above, the pixel brightness level is a reflection of the intensity of the signal coming from the tested object. This intensity changes with changes in TE and TR.

Let us return to Equation 2 and assume the TE value to be as small as possible at the level of a few milliseconds. Then the component of equation will be close to the value 1.

$$\lim_{TR \rightarrow 0} \left(PD \left(1 - e^{-\frac{TR}{T_1}} \right) e^{-\frac{TR}{T_2}} \right) = PD \left(1 - e^{-\frac{TR}{T_1}} \right) \text{ Equation 3} \quad \text{Equation 3}$$

This will cause the measured IS magnetic resonance signal to be approximately dependent only on the T_1 value. In order to determine the relaxation time T_1 , it is necessary to find the value on the X axis at which IS reaches 63% of the maximum value. The value of 63% is not a random value but sets a point on the timeline at which $TR = T_1$ and thus gives the expression:

$$\left(1 - e^{-\frac{TR}{T_1}} \right)_{TR=T_1} \approx 0.63212 \approx 63\% \quad \text{Equation 4}$$

Practically speaking, to determine the T_1 time, it is necessary to register a series of images of the examined object by changing the TR value in the whole range of its variability followed by reading the IS signal intensity value for the region of interest (ROI) and plotting the curve to find a point 63% of the maximum value. It should be noted that increasing the number of measuring points will contribute to a more accurate determination of the sought value. When making measurements, temperature stability is important because the time T_1 is directly related to it. Performing this operation for each pixel, it is possible to draw an image that will illustrate the distribution of T_1 times in the studied area.

We can present a similar reasoning to determine the transverse relaxation time T_2 . Figure 1b shows examples of T_2 relaxation time charts. To this end, let us suppose that TR is large compared to the value of T_1 , then the IS will be proportional to:

$$\lim_{TR \rightarrow \infty} \left(PD \left(1 - e^{-\frac{TR}{T_1}} \right) e^{-\frac{TR}{T_2}} \right) = PD e^{-\frac{TR}{T_2}} \quad \text{Equation 5}$$

The determination of time T_2 consists of determining a point on the time axis at which the IS drops to 37%. Equation 5 will only take this value when $TE = T_2$.

$$\left(e^{-\frac{TE}{T_2}} \right)_{TE=T_2} \approx 0.36788 \approx 37\% \quad \text{Equation 6}$$

The algorithm describing the principle of measuring time T_2 is also based on recording images but with changing TE from the smallest possible available in the system. TR should be set as high as possible. Keep in mind that increasing the TR time can directly affect the extension of the sequence time. For in vitro tissue testing, this is not particularly important, except in some cases, but for patient testing this is essential. The character of the chart is exponential, which shows large changes in a narrow range of TE changes. For the correct determination of this value, a large number of measuring points are necessary. This treatment allows for reduction of the error associated with determining this time because it allows adjustment the approximation curve more accurately. In addition to the T_2 time,

there is also a parameter called T_2^* . These two parameters are similar, but there are differences that cannot be ignored. Time T_2^* depends on the device and the patient and is defined by Equation 7.

$$\frac{1}{T_2^*} = \frac{1}{T_2} + \frac{1}{T_2'} \quad \text{Equation 7}$$

$$R2^* = R2 + R2'$$

Time T_2^* depends on, and results from, the heterogeneity of the magnetic field.

In Equation 2, there is one more factor that has not been mentioned until now, namely proton density (PD). It is a quantity describing the hydrogen content in the tissue. It is directly proportional to the number of hydrogen atoms. For this reason, PD will be high in fluids and low in solid tissues. This is a parameter that cannot be ignored in MR imaging. However, you can choose the image received depending on the TE and TR times. The result of PD-dependent imaging will be the distribution of hydrogen atoms in the test space. In order for this effect to occur, the scanner must have TE as short as possible and long TR. Then the relationships described by Equation 3 and 5 will occur simultaneously, so the signal will depend in practice only on PD, with very small influences of T_1 and T_2 . Measurements of cell culture relaxation times are another class of study due to the lack of the need to shorten the study time as it is in the case of patient studies. It is also difficult to use MOLLI, ShMOLLI, SASHA, or other methods due to the natural lack of the possibility of ECG gating [18–21]. Both T_1 and T_2 are the time after which longitudinal and transverse relaxation, respectively, reach certain well-defined values. The basic methods of measuring these parameters are: saturation and regrowth (SR), reversal and regrowth (IR), and spin echo (SE) methods [5]. An important regularity is that in the T_1 -dependent test, the signal from a given tissue is inversely proportional to the T_1 time of that tissue. It is different in the case of T_2 -dependent imaging, namely the tissue signal is proportional to its time T_2 .

The method for measuring these times is to perform a series of sequences with changing TE and TR parameters, and measure in the region of interest (ROI) the value of the received signal intensity. This is done by determining the average value of the already reconstructed image of the layer and plotting these values on the chart. On the horizontal axis there are values of the changing times TR for the measurement T_1 or also TE for T_2 . The result of the work are graphs analogous to those shown in Figure 1. Their character coincides with the longitudinal magnetisation M_z reconstruction charts. To increase the accuracy of determining relaxation times it is necessary to approximate the obtained results with the function describing the given curve. The phenomenon of relaxation is determined by relatively

simple mathematical relationships, which results in relatively easy function analysis and determination of the approximating function. Knowing the approximating function, you can readily determine T_1 and T_2 .

It should be borne in mind that by determining IS at different points in the test space and thus different distances from the coil we will get different maximum values. It is therefore necessary to approximate the received signal to $<0.1>$ before approximation. The normalisation procedure will therefore minimise errors related to the effect of signal intensity as a function of distance from the receiving coil. Despite the low complexity of the approximating functions, it is advisable that the number of sequences performed with the appropriate changes in TE and TR times is as large as possible, so that the effects affecting measurement errors are minimised. And so, from the author's experience, it appears that matching at the level of $R^2 > 0.98$ is obtained for 8-10 measuring points for T_1 times, while for T_2 the number of points should be the same or greater. The number of these points is similar both for tissues and for homogeneous samples (liquids). When choosing TE time and TR time values in tests, one should be guided by the fact that not only the IS value but also its shape as a function of the set times are subject to mathematical analysis. It cannot be overestimated in determining T_1 , it turns out to know the IS value for very long TR times of 12000-15000 ms – then the measured value determines the maximum value. The consequence of sequences with such long times is a significant extension of the test time, which is not always acceptable. Determining the T_2 value is a bit more complicated in this respect. It is necessary to know the maximum signal value that occurs at minimum TE times at the level of single milliseconds. An attempt to obtain an image from such a set sequence may fail due to the fact that not every magnetic resonance imaging scanner will allow such

low values of the echo time. In addition, the IS graph in the TE function for long times flattens at a certain level, which should be considered as the background and subtracted. The shape of the falling curve is still interesting; not its absolute value but determination when it reaches 37% of the maximum value.

In the theoretical part of this study, diagrams and the SR method for determining times T_1 and T_2 are shown. This is the most intuitive method and was quoted for easier understanding of the very idea of measurement. As mentioned before, the second method is the reversal and regrowth (IR) method. The difference from the SR method is that the first 180° pulse is used instead of 90° . Equation describing the behaviour of the magnetisation vector M_z (Fig. 9).

The characteristic points are the zero-crossing points of the magnetisation characteristic. In MR imaging, by selecting the inversion time (TI) in the magnetic resonance scanner at 69.3% of the T1 time for a specific tissue, it can be eliminated from the image.

The T_1 value can be determined from the formula:

$$T_1 = \frac{-t}{\ln \frac{1}{2}} \quad \text{Equation 9}$$

An interesting concept for measuring T_1 and T_2 tissue times has been proposed by the authors [6]. The authors proposed using images obtained in four sequences at the TE and TR times defined. This method seems to be a very attractive way of determining relaxation times due to the short time of examination, but attention should be paid to the fact that it is very sensitive to errors. Even the smallest errors with such a small number of measuring points can lead to large scatter in the results obtained. It should be remembered that relaxation time courses are exponential functions and therefore strongly non-linear. Researchers conducted their work using three phantoms, which are dissolved

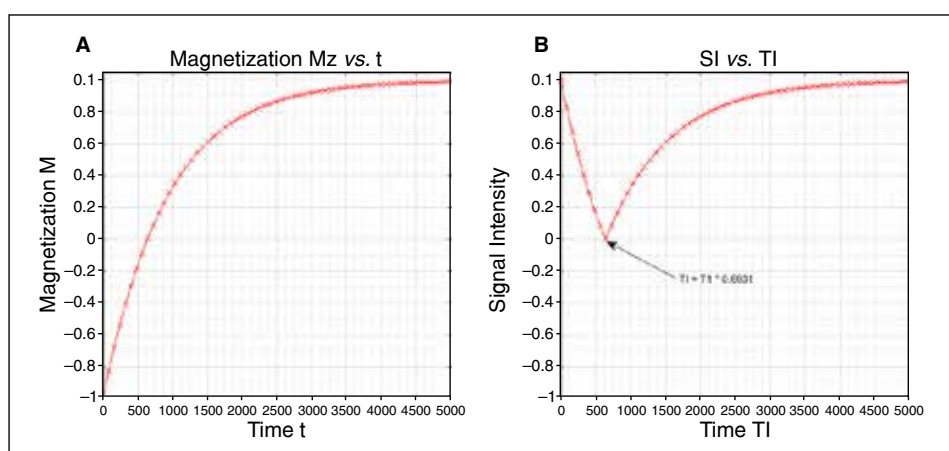


Figure 9. Graphs of magnetization M_z (A) and signal intensity depending on time TI (B)

gadolinium saline. Such a phantom is a homogeneous phantom. Magnetic resonance tomography, like any other type of tomography, assumes homogeneity of the medium in a given voxel. In contrast to homogeneous fluids in the body of the examined patient, there is no such homogeneity. Minimal movement of the test tissue and hence the wrong measurement of the signal intensity should always be taken into account. Measurement of intensity takes place in the area commonly known as the ROI.

If we assume that for calculations we will always take the same area in the image, and the result of the test will shift the examined structures, and the ROI will accidentally find adjacent tissues not covered by measurement in other sequences, this may lead to falsification of the IS value and thus increase the uncertainty of the relaxation time measurement result. Analysing the work of various authors, many solutions can be found to increase the speed of obtaining the T_1 times [7-9, 11-14]. The vast majority of them, however, essentially use SR or IR methods. A completely different method was proposed in an article by Wang [10]. Their innovative approach to determining T_1 relaxation time is a real fusion of two methods: ST and IR. According to the authors, this method known by the abbreviation SIR – saturation-inversion-recovery – allows the T_1 time value to be obtained with much higher resolution compared to the SR and IR methods. Their development is used especially where there is a need to differentiate areas with similar T_1 time values where this resolution is limited. Magnetic resonance tomography, like any method of this type, assumes a homogeneous structure in the test space. In fact, this is not the case because we usually deal with complex substances, each of which has its own time T_1 . When measuring the relaxation time, averaging is performed and the T_1 time value is the result of the relaxation time in a given area.

Relaxation times are the basic parameters that characterise the examined objects in magnetic resonance imaging. In recent years, leading manufacturers of magnetic resonance imaging systems have included in their portfolio a number of applications that illustrate anatomy using relaxation times. Obtained images of the myocardium, brain areas, and neoplastic lesions where the T_1 or T_2 time values are colour coded have given doctors an additional diagnostic tool significantly affecting medical diagnostics. The latest software allows post-processing changes of TE, TR, and TI times, which makes it possible to obtain several images, including parametric images (T_1 , T_2 , STIR, T_1 FLAIR, T_2 FLAIR, PD) in a significantly shorter time. Nevertheless, at the core of this technology are the principles of measuring relaxation times with in-depth knowledge of phenomena affecting the accuracy of the results obtained. The conducted experiments show that the protocols that were

created for imaging the structures of the human body do not always give correct results for cell cultures. It is therefore necessary to modify them to select optimal scanning conditions. The second important conclusion is that the MCF-7 tumour cells have a shorter T_1 time compared to the normal HMEC cells.

Abbreviations: MRI – magnetic resonance imaging; MRS – magnetic resonance spectroscopy; PD – proton density in tissue; T_1 – longitudinal relaxation time tissue; T_2 – transverse relaxation time tissue; TE – echo time; TR – repetition time

Acknowledgments:

Dorota Bartusik-Aebisher acknowledges support from the National Center of Science NCN (New drug delivery systems-MRI study, Grant OPUS-13 number 2017/25/B/ST4/02481).

References

- Rabi I, Zacharias JR, Millman S, et al. Milestones in magnetic resonance: 'a new method of measuring nuclear magnetic moment' . 1938. *J Magn Reson Imaging*. 1992; 2(2): 131–133, doi: [10.1002/jmri.1880020203](https://doi.org/10.1002/jmri.1880020203), indexed in Pubmed: [1562763](https://pubmed.ncbi.nlm.nih.gov/1562763/).
- Walecki J, Ziemiański A. Rezonans magnetyczny i tomografia komputerowa w praktyce klinicznej. Springer PWN, Warszawa. ; 1998: 12–21.
- Mirhej ME. PROTON SPIN RELAXATION BY PARAMAGNETIC MOLECULAR OXYGEN. *Canadian Journal of Chemistry*. 1965; 43(5): 1130–1138, doi: [10.1139/v65-150](https://doi.org/10.1139/v65-150).
- Rummeny EJ, Reimer P, Heindel W. Obrazowanie ciała metodą rezonansu magnetycznego. ; 2010: 1–6.
- Elmaoglu M, Celik A. Rezonans magnetyczny podstawy fizyczne obrazowanie ułożenie pacjenta Protokoly. Medipage. ; 2015: 1–9.
- Zhang L, Zhang Z, Mason RP et al. Convertible MRI contrast: Sensing the delivery and release of anti-glioma nano-drugs. *Sci Rep*. 2015; 5: 9874, doi: [10.1038/srep09874](https://doi.org/10.1038/srep09874), indexed in Pubmed: [25962872](https://pubmed.ncbi.nlm.nih.gov/25962872/).
- Yang DM, Huettner JE, Bretthorst GL, et al. Intracellular water preexchange lifetime in neurons and astrocytes. *Magn Reson Med*. 2018; 79(3): 1616–1627, doi: [10.1002/mrm.26781](https://doi.org/10.1002/mrm.26781), indexed in Pubmed: [28675497](https://pubmed.ncbi.nlm.nih.gov/28675497/).
- Shi Y, Guenneau F, Wang X, et al. MnO-gated Nanoplatfoms with Targeted Controlled Drug Release and Contrast-Enhanced MRI Properties: from 2D Cell Culture to 3D Biomimetic Hydrogels. *Nanotheranostics*. 2018; 2(4): 403–416, doi: [10.7150/ntno.28046](https://doi.org/10.7150/ntno.28046), indexed in Pubmed: [30324085](https://pubmed.ncbi.nlm.nih.gov/30324085/).
- Bartusik D, Tomanek B. Detection of (19F)-labeled biopharmaceuticals in cell cultures with magnetic resonance. *Adv Drug Deliv Rev*. 2013; 65(8): 1056–1064, doi: [10.1016/j.addr.2013.04.010](https://doi.org/10.1016/j.addr.2013.04.010), indexed in Pubmed: [23603212](https://pubmed.ncbi.nlm.nih.gov/23603212/).
- Wang H, Zhao M, Ackerman JL, et al. Saturation-inversion-recovery: A method for T measurement. *J Magn Reson*. 2017; 274: 137–143, doi: [10.1016/j.jmr.2016.11.015](https://doi.org/10.1016/j.jmr.2016.11.015), indexed in Pubmed: [27918897](https://pubmed.ncbi.nlm.nih.gov/27918897/).
- Fanea L, Sfrangeu SA. Relaxation times mapping using magnetic resonance imaging. *Roman Rep Phys*. 2011; 63(2): 456–464.
- Gonet B. Obrazowanie magnetyczno-rezonansowe, Wydawnictwo Lekarskie PZWL Warszawa. ; 1997: 11–45.
- Treier R, Steingoeetter A, Goetze O, et al. Fast and optimized T1 mapping technique for the noninvasive quantification of gastric secretion. *J Magn Reson Imaging*. 2008; 28(1): 96–102, doi: [10.1002/jmri.21400](https://doi.org/10.1002/jmri.21400), indexed in Pubmed: [18581398](https://pubmed.ncbi.nlm.nih.gov/18581398/).

14. Hsu JJ, Glover GH. Rapid MRI method for mapping the longitudinal relaxation time. *J Magn Reson.* 2006; 181(1): 98–106, doi: [10.1016/j.jmr.2006.03.014](https://doi.org/10.1016/j.jmr.2006.03.014), indexed in Pubmed: [16621631](https://pubmed.ncbi.nlm.nih.gov/16621631/).
15. Hsu JJ, Zaharchuk G, Glover GH. Rapid methods for concurrent measurement of the RF-pulse flip angle and the longitudinal relaxation time. *Magn Reson Med.* 2009; 61(6): 1319–1325, doi: [10.1002/mrm.21900](https://doi.org/10.1002/mrm.21900), indexed in Pubmed: [19267342](https://pubmed.ncbi.nlm.nih.gov/19267342/).
16. Hirasaki GJ, Lo SW, Zhang Y. NMR properties of petroleum reservoir fluids. *Magn Reson Imaging.* 2003; 21(3-4): 269–277, doi: [10.1016/s0730-725x\(03\)00135-8](https://doi.org/10.1016/s0730-725x(03)00135-8), indexed in Pubmed: [12850718](https://pubmed.ncbi.nlm.nih.gov/12850718/).
17. Franks F. *Water a comprehensive treatise. The physics and physical chemistry of water*, plenum-press, New. ; 1972: 235–237.
18. Piechnik SK, Ferreira VM, Dall'Armellina E, et al. Shortened Modified Look-Locker Inversion recovery (ShMOLLI) for clinical myocardial T1-mapping at 1.5 and 3 T within a 9 heartbeat breathhold. *J Cardiovasc Magn Reson.* 2010; 12: 69, doi: [10.1186/1532-429X-12-69](https://doi.org/10.1186/1532-429X-12-69), indexed in Pubmed: [21092095](https://pubmed.ncbi.nlm.nih.gov/21092095/).
19. Cooper MA, Nguyen TD, Spincemaille P et al. How accurate is MOLLI T1 mapping in vivo? Validation by spin echo methods. *PLoS One.* 2014; 9(9): e107327, doi: [10.1371/journal.pone.0107327](https://doi.org/10.1371/journal.pone.0107327), indexed in Pubmed: [25211243](https://pubmed.ncbi.nlm.nih.gov/25211243/).
20. Weingärtner S, Meßner NM, Budjan J, et al. Myocardial T-mapping at 3T using saturation-recovery: reference values, precision and comparison with MOLLI. *J Cardiovasc Magn Reson.* 2016; 18(1): 84, doi: [10.1186/s12968-016-0302-x](https://doi.org/10.1186/s12968-016-0302-x), indexed in Pubmed: [27855705](https://pubmed.ncbi.nlm.nih.gov/27855705/).
21. Hamdy A, Kitagawa K, Ishida M, et al. Native Myocardial T1 Mapping, Are We There Yet? *Int Heart J.* 2016; 57(4): 400–407, doi: [10.1536/ihj.16-169](https://doi.org/10.1536/ihj.16-169), indexed in Pubmed: [27396560](https://pubmed.ncbi.nlm.nih.gov/27396560/).
22. Heidenreich JF, Weng AM, Donhauser J, et al. T1- and ECV-mapping in clinical routine at 3T: differences between MOLLI, ShMOLLI and SASHA. *BMC Med Imaging.* 2019; 19(1): 59, doi: [10.1186/s12880-019-0362-0](https://doi.org/10.1186/s12880-019-0362-0), indexed in Pubmed: [31370821](https://pubmed.ncbi.nlm.nih.gov/31370821/).
23. Chow K, Flewitt JA, Green JD, et al. Saturation recovery single-shot acquisition (SASHA) for myocardial T(1) mapping. *Magn Reson Med.* 2014; 71(6): 2082–2095, doi: [10.1002/mrm.24878](https://doi.org/10.1002/mrm.24878), indexed in Pubmed: [23881866](https://pubmed.ncbi.nlm.nih.gov/23881866/).
24. Costello BT, Springer F, Hare JL, et al. SASHA versus ShMOLLI: a comparison of T1 mapping methods in health and dilated cardiomyopathy at 3 T. *Int J Cardiovasc Imaging.* 2017; 33(10): 1551–1560, doi: [10.1007/s10554-017-1134-y](https://doi.org/10.1007/s10554-017-1134-y), indexed in Pubmed: [28589482](https://pubmed.ncbi.nlm.nih.gov/28589482/).
25. Nordio G, Henningsson M, Chiribiri A, et al. 3D myocardial T mapping using saturation recovery. *J Magn Reson Imaging.* 2017; 46(1): 218–227, doi: [10.1002/jmri.25575](https://doi.org/10.1002/jmri.25575), indexed in Pubmed: [28152227](https://pubmed.ncbi.nlm.nih.gov/28152227/).